Supersonic Separated and Reattaching Laminar Flows: I. General Theory and Application to Adiabatic Boundary-Layer/Shock-Wave Interactions

LESTER LEES* AND BARRY L. REEVES†
California Institute of Technology, Pasadena, Calif.

This paper deals with laminar boundary-layer/shock-wave interactions in which the pressure rise generated in an "external" supersonic, inviscid flow is communicated upstream through the boundary layer and thereby induces flow separation. In order to describe this phenomenon approximately, including the subsequent reattachment of the flow, we utilize an integral or moment method in which the first moment of momentum is employed, in addition to the usual momentum integral (zeroth moment). By this means, the velocity and enthalpy profiles are characterized by a single independent parameter not explicitly related to the local static pressure gradient. The present theoretical calculations agree quite well with the adiabatic laminar boundary-layer/shock-wave interaction experiments of Chapman and Hakkinen and the experimental results of Sterrett and Emery on the "free interaction" upstream of a forward facing step. Calculations for highly cooled surfaces are in progress and will be reported as Part II (which will be submitted for publication at a later date). The limitations of the two-moment method based on a one-parameter family of velocity profiles are discussed and the role of a two-moment, two-parameter method such as Wieghardt's is examined briefly. We remark that the general theory developed here is also applicable to base flows and wake flows.

Nomenclature

a = speed of sound; also velocity profile parameter $[\partial(U/U_e)/\partial(Y/\delta_i)]_{Y=0}$ for attached flow; $(Y/\delta_i)_{U/U_e=0}$ for separated flow
B = $\{\mathcal{H} + [(1 + m_e)/m_e]\}$
c_v, c_p = specific heat at constant volume and constant pressure, respectively
$D(\mathcal{H}, M_e)$ = function defined in Eq. (22a)
e = enthalpy integral defined in Eq. (7d)
E = integral defined in Eq. (7e)
f = $2\mathcal{H} + \frac{3\gamma - 1}{\gamma - 1} + \frac{\gamma + 1}{\gamma - 1}\left(\frac{m_e}{1 + m_e}\right)\mathcal{H} + \frac{(M_e^2 - 1)}{m_e(1 + m_e)}Z$
h = static enthalpy; also function defined in Eq. (17)
h_s = total enthalpy
$\mathcal{H}$ = θ_i/δ_t^*
J = θ_i^*/δ_t^*
m = $[(\gamma - 1)/2]M^2$
M = Mach number
N_1, N_2, N_3 = functions defined in Eqs. (22b–22d)
p = pressure
P = wall shear stress function, $(\delta_t^*/U_e)(\partial U/\partial Y)_{Y=0}$
Pr = Prandtl number
R = dissipation function, $(2\delta_t^*/U_e^2)\int_0^{\delta_i}\left(\frac{\partial U}{\partial Y}\right)^2 dY$
Re_{δ^*} = $[(u_e\delta^*)/\nu_e]$
$\tilde{R}e_{\delta_t^*}$ = $[(a_\infty M_e\delta_t^*)/\nu_\infty]$ } Reynolds numbers
$Re_{x,0}$ = $[(u_e x_0)/\nu_e]_{\infty-}$

S = total enthalpy function, $(h_s/h_{s_e}) - 1$
T^* = enthalpy function, $E/(S_w\delta_t^*)$
u, v = velocity components parallel and normal to surface, respectively
u^* = velocity ratio along dividing streamline, $(u/u_e)_\psi = 0$
U = Stewartson's transformed velocity, $u(a_\infty/a_e)$
x, y = coordinates parallel and normal to surface, respectively
X, Y = Stewartson's transformed coordinates [Eq. (1)]
Z = velocity integral, $(1/\delta_t^*)\int_0^{\delta_i}\left(\frac{U}{U_e}\right)dY$
β = Falkner-Skan pressure gradient parameter
γ = ratio of specific heats, (c_p/c_v)
δ = boundary-layer thickness
δ_i = transformed boundary-layer thickness
δ^* = boundary-layer displacement thickness [Eq. (7a)]
δ_t^* = transformed displacement thickness, $\delta_i^* + e$
ϵ = $M_e - M_{\infty\pm}$
η = similarity variable, $Y([(m + 1)/2](U_e/\nu_0 X))^{1/2}$
θ = boundary-layer momentum thickness [Eq. (7b)]
θ^* = mechanical "energy" thickness [Eq. (7c)]
Θ = local angle between "external" streamline at $y = \delta$ and x axis $\tan^{-1}(v_e/u_e)$
κ = Crocco-Lees profile parameter
Λ = Pohlhausen parameter
μ = viscosity
ν = Prandtl-Meyer angle; also kinematic viscosity (μ/ρ)
ρ = gas density
τ = shear stress
ψ = stream function

Subscripts

b = Blasius
e = local "external" inviscid
i = transformed
s = separation point
w = wall
x = along plate
0 = beginning of interaction
∞, $\infty-$ = far upstream of shock
$\infty+$ = far downstream of shock

Presented as Preprint 64-4 at the AIAA Aerospace Sciences Meeting, New York, January 20–22, 1964; revision received July 13, 1964. The work discussed in this paper was carried out under the sponsorship and with the financial support of U. S. Air Force, Grant No. AF-AFOSR-54-63. This paper supercedes Graduate Aeronautical Laboratory, California Institute of Technology, Separated Flows Project Technical Report 3 (October 4, 1963).

* Professor of Aeronautics. Fellow Member AIAA.
† Research Fellow; now with Research and Development Division, Avco Corporation, Wilmington, Mass. Member AIAA.

1. Introduction

IN the usual formulation of the Prandtl boundary-layer theory, the static pressure distribution along the surface is given by the inviscid flow over the surface in the absence of a boundary layer. There is an important class of viscous flows, however, in which the static pressure distribution is not a given datum of the problem, but is determined by the interaction between the "external" inviscid flow and the viscous layer near the surface. Prandtl[1] himself described boundary-layer flow separation in these terms; "strong interaction" in hypersonic viscous flow[2, 3] is a more recent example. One of the most intriguing viscous-inviscid interactions is the boundary-layer separation induced by a static pressure rise in an "external" supersonic flow that is communicated upstream through the boundary layer itself. This pressure rise may be generated by an incident oblique shock, for example, or by a corner. Ackeret, Feldman, and Rott[4] first observed this phenomenon in the imbedded supersonic region over an airfoil at transonic speeds. All the main features of the flow pattern are strikingly delineated in the beautiful schlieren studies of Liepmann.[5] Following earlier theoretical work on this type of problem by Oswatitsch and Wieghardt,[6] the senior author[7] gave a theoretical explanation of the extensive region of upstream influence for adiabatic flow and showed that the overpressure on the surface decays exponentially with distance upstream of the separation point. However, this study did not succeed in dealing with the viscous flow downstream of separation and its subsequent reattachment. In fact, until recently, the only theoretical treatment of reattachment worth mentioning was Chapman's[8] analysis for the particular case of zero boundary-layer thickness "far" upstream of the reattachment point.

In spite of the long-time interest in the boundary-layer/shock-wave interaction problem, a satisfactory theoretical analysis does not yet exist. Some theoretical studies employ a modified Kármán-Pohlhausen method, without much success[9, 10]; others utilize a two-moment method, but are forced to patch together the preseparation and postseparation regions by means of various ad hoc techniques[11, 12]; still others utilize a plausible but semiempirical mixing or mass entrainment rate between the inviscid and viscous flows.[13–15] The situation is particularly unsatisfactory for flows with heat transfer. The aim of the present paper is to construct a theory that is capable of including the entire flow within a single framework, without introducing semiempirical features.

Provisionally we make the assumption that the boundary-layer approximations are valid over the entire viscous flow region; the self-consistency of this assumption must be checked a posteriori. Once this working hypothesis is adopted, integral or moment methods are quite attractive for viscous-inviscid interaction problems. In the present study, we employ the first moment of the momentum in addition to the usual momentum integral (zeroth moment). This method itself is not new,[11, 12, 16–18] but it turns out that its successful application to separated and reattaching flows hinges on the proper choice of the one-parameter family of velocity profiles utilized to represent the integral properties of the viscous flow. We show that the Stewartson[19] reversed-flow profiles and their Cohen-Reshotko[20] analogs for flows with heat transfer have the qualitatively correct behavior; polynomials do not.

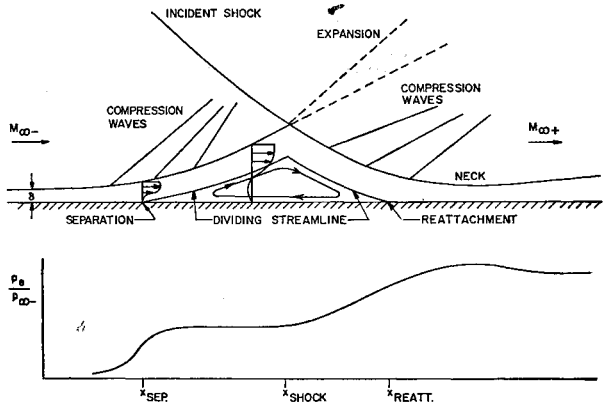

Fig. 1 Schematic representation of shock-wave/laminar-boundary-layer interaction.

Section 2 contains a physical description of the flow pattern, a summary of the main features of the two-moment method, and the reasons for the selection of the Stewartson family of velocity profiles. In Sec. 3, the general mathematical theory is developed, including flows with heat transfer, and the distinction between "supercritical" and "subcritical" flows is brought out. In Sec. 4, the theory is applied to adiabatic boundary-layer/shock-wave interaction, and the results are compared with the experiments of Chapman et al.,[8] and Hakkinen et al.,[21] and Sterrett and Emery.[22] The limitations of the two-moment method based on a one-parameter family of velocity profiles are discussed in Sec. 5, and some brief remarks on the extension of the present method to base flows and wake flows are contained in Sec. 6.

This paper constitutes Part I of this study; Part II will contain numerical solutions for flows with heat transfer.

2. Model of Supersonic Separated and Reattaching Laminar Flows

2.1 Description of the Flow

The interaction between an incident oblique shock wave and the laminar boundary layer on a flat plate is represented schematically in Fig. 1. The positive pressure disturbance caused by the shock propagates upstream through the subsonic portion of the boundary layer. Unless the shock wave is very weak, the laminar boundary layer separates from the surface upstream of shock impingement.[7] At the separation point, the "dividing streamline" leaves the surface at a definite angle, according to Oswatitsch.[23] The flow above this streamline includes all the fluid contained in the boundary layer just upstream of separation; below this streamline, a steady, recirculating flow is trapped in the roof-shaped "bubble" between the separation and reattachment points (Fig. 1). Because of the transfer of momentum from the "external" inviscid stream to the viscous flow above the dividing streamline, the velocity ratio $(u/u_e)_{\psi=0}$ along this streamline increases continuously in the downstream direction. By this process, the flow is prepared for the additional pressure rise during reattachment.[8, 15] As the viscous layer thickens downstream of separation, the positive pressure gradient steadily decreases, until the famous "pressure plateau"[8, 21] is reached just upstream of shock impingement (Fig. 1).

The subsonic portion of the viscous layer cannot support a sudden pressure rise; therefore, the incident shock is reflected as an expansion fan that just cancels the pressure jump across the shock. Because of this reflection condition, the flow at the outer edge of the viscous layer is suddenly deflected toward the plate surface (Fig. 1). The viscous layer is squeezed against the surface and forced to turn as it flows downstream, and this turning produces a pressure rise and deceleration of the flow in the viscous layer. More and more fluid below the dividing streamline is turned back as the flow proceeds downstream, until the velocity along this streamline itself is brought to rest at the reattachment point (Fig. 1). Downstream of this point, the fluid above the dividing streamline forms a new boundary layer. This layer reaches a minimum section, or "neck," before relaxing to the "normal" state corresponding to a weak, supersonic viscous interaction at the new Mach number.

This description of laminar boundary-layer/shock-wave interaction is based on our understanding of the more familiar adiabatic case. In this case, the viscous flow is entirely "subcritical" in the sense that the pressure rise generated by the incident shock is communicated smoothly all the way upstream to the "initial" flat-plate flow, as in a subsonic nozzle flow. Crocco[24] found that $(d\delta/dp) > 0$ in such flows, whereas in a "supercritical" flow $(d\delta/dp) < 0$. Thus, a subcritical boundary layer is capable of generating its own positive pressure gradient in the flow direction by interacting with an external, inviscid supersonic stream. A supercritical flow, on the other hand, responds to a pressure rise generated downstream only through a sudden "jump" or "shock" to a subcritical state.[24]‡ Downstream of this jump the flow proceeds smoothly. The analogy to a supersonic nozzle flow is clear; the viscous flow behaves as if some equivalent average Mach number is "supersonic."

Within the framework of the Crocco-Lees[13] mixing theory, adiabatic laminar boundary layers are subcritical, whereas adiabatic turbulent boundary layers are supercritical.[24, 25] This property partly accounts for the qualitatively different behavior of laminar and turbulent boundary-layer/shock-wave interactions. Crocco[24] mentioned briefly that adiabatic laminar boundary layers could go supercritical in a negative pressure gradient. In this paper we investigate the conditions under which laminar boundary layers may be supercritical within the present theoretical framework, and we examine some of the interesting consequences of this behavior (Sec. 3.2).

2.2 Integral Methods of Solution

Because of the complexity of this problem, all the known approaches utilize integral or moment methods that describe the flow in some average sense. Gadd[9] and Curle[10] employed a modified Kármán-Pohlhausen method that is actually an extension of Thwaites' technique.[26, 27] For the separated flow region, they utilized Stewartson's[19] "lower branch" solutions of the Falkner-Skan equation to obtain the skin-friction and "form parameter" function appearing in Thwaites' formulation of the boundary-layer momentum equation. However, their results do not show the well-known pressure plateau downstream of separation, so their static pressure rise at shock impingement is considerably higher than the experimentally observed value (cf. Fig. 5 of Ref. 10). Martellucci and Libby[28] utilized an even simpler approach for the adiabatic case, based on the original Pohlhausen quartic velocity profiles, with similar results.

The chief defect of the Kármán-Pohlhausen method is that the velocity profile and all the integral properties of the flow are uniquely determined by the local static pressure gradient. Along the pressure plateau, for example, the pressure gradient is virtually zero, but the velocity profiles are certainly not "similar"; they coincide neither with the Blasius flow nor with Stewartson's limiting reversed-flow profile (see Sec. 2.3). In order to avoid this difficulty, the method devised by Crocco and the senior author[13] utilized a shape parameter $\varkappa(x)$ that is not explicitly related to the local pressure gradient or to the momentum thickness θ. If the zeroth moment or momentum integral is employed, and no higher moments, a second relation is required in order to determine the behavior of the two independent quantities $\varkappa(x)$ and $\theta(x)$. This relation is supplied by specifying the "mixing rate" or rate of mass entrainment from the external inviscid flow.[13] For attached viscous layers, this relation offers no difficulty in principle, but the extension to separated and reattaching flows is necessarily semiempirical.

Glick[15] made significant improvements in the Crocco-Lees method, especially in the specification of the mixing rate function. He showed that previous quantitative disagreements between theory and experiment[14] in the region upstream of separation could be attributed to an incorrect mixing rate function $C(\varkappa)$ based on the Falkner-Skan similar solutions. These solutions do not properly account for the history of the boundary-layer flow as far as mixing is concerned. When $C(\varkappa)$ is based on a suitable average of experimental data and theoretical calculations that include flow history, excellent agreement is obtained between predicted and measured surface pressure distributions upstream of separation. In the region between separation and shock impingement, Glick[15] determined the mixing rate function by matching the predicted pressure distribution upstream of separation with the results of a single experiment. When this mixing rate is applied to another experiment at about the same Mach number, but at a Reynolds number ten times higher, agreement between theory and experiment is quite satisfactory. The "dip" in static pressure between separation and shock impingement and other anomalies found by Bray, Gadd, and Woodger[14] are totally eliminated. However, one has no way of knowing in advance whether Glick's semiempirical function can be extended to higher Mach numbers or to flows with heat transfer.

In order to avoid the semiempirical features of the Crocco-Lees method for separated and reattaching flows, at least one additional moment of the momentum equation must be employed. This idea seems to recur constantly in boundary-layer theory; it was proposed by Sutton,[16] by Walz,[17] and most recently by Tani.[18] Tani specifies the velocity profiles in terms of a single independent parameter $a(x)$ proportional to the slope at the surface. By abandoning the condition on $(\partial^2 u/\partial y^2)$ at the plate surface and utilizing the zeroth and first moments of the momentum equation, he obtains two simultaneous, first-order, ordinary nonlinear differential equations for $a(x)$ and $\theta(x)$. Tani's method gives excellent agreement with "exact solutions" for prescribed adverse pressure gradients.[18] The present authors have shown[30] that Tani's method is also quite suitable for describing a nonsimilar "relaxation" of the boundary-layer flow, even for uniform static pressure.

When Abbott, Holt, and Nielsen[12] applied Tani's method to the boundary-layer/shock-wave interaction problem, they found good agreement between theory and experiment for adiabatic flow up to separation. However, except at very low Reynolds numbers, their calculations showed a physically unrealistic static pressure maximum on the plate surface downstream of separation. This maximum in the static pressure is even more pronounced for cooled boundary layers $(S_w < 0)$. In addition, the thermal energy downstream of separation flows in the wrong direction at the surface; the cooled surface is heating the boundary layer! For $(h_w/h_{s_e}) < 0.55$ at $M_\infty = 4$, no solutions at all could be found.

All of the difficulties experienced by Abbott, Holt, and Nielsen are caused primarily by the use of Tani's quartic velocity profiles (Secs. 2.3, 4.1, and 5). In the present report, the attractive features of Tani's technique are combined with the more appropriate Stewartson[19] reversed-flow profiles. In addition, we adopt the simplest possible procedure for the total enthalpy profile and link it to the velocity profile parameter $a(X)$ and the value of S_w through the Cohen-Reshotko[20] analogs of Stewartson's solutions (Sec. 2.3). In this manner we make certain that the total enthalpy profile and the direction of heat flux at the surface are qualitatively correct over the entire interaction zone, including reattachment.

2.3 Velocity and Enthalpy Profiles

Downstream of separation, the magnitude of the peak reversed-flow velocity in the viscous layer increases steadily with distance along the surface, reaches a maximum, and then decreases again as the dividing streamline moves farther

‡ Of course this jump must be interpreted as a rapid change in flow quantities over a distance of one or two boundary-layer thicknesses.

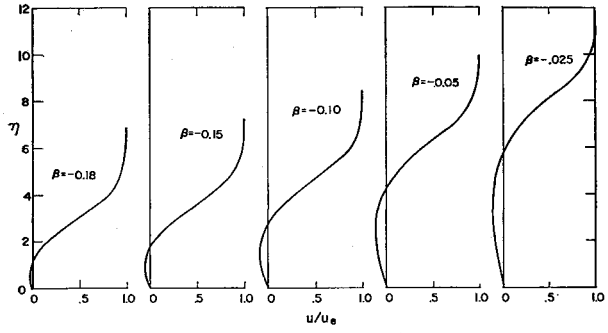

Fig. 2a Stewartson reversed-flow profiles for low-speed, isothermal flow.

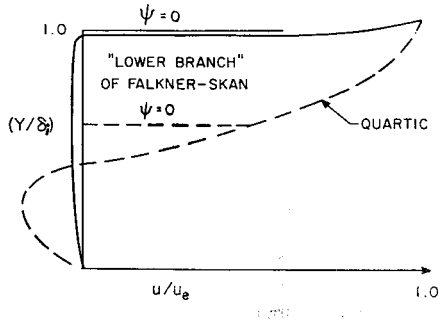

Fig. 2b Comparison of similarity velocity profiles in separated flow for vanishingly small adverse pressure gradient.

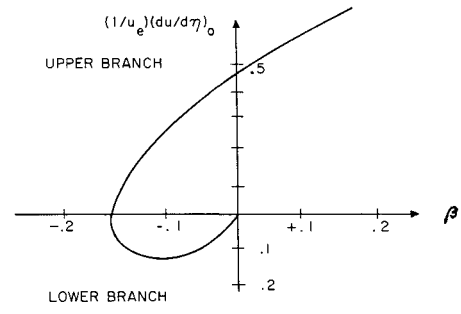

Fig. 2c Slope of velocity profile at surface for Falkner-Skan solutions.

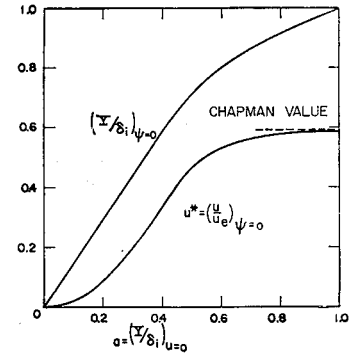

Fig. 2d Characteristics of separated flow velocity profiles

and farther away from the surface (Fig. 1). A polynomial representation of the velocity profile based on a single parameter is clearly inadequate to describe this sequence of events. On the other hand, the reversed-flow solutions found by Stewartson[19] along the "lower branch" of the Falkner-Skan family have the qualitatively correct behavior, provided one "unhooks" the velocity profiles from the pressure gradient parameter β (Fig. 2a).

As an illustration, consider the "similar" solution for separated flow in the limiting case of zero pressure gradient found in Ref. 30 by utilizing the two-moment method plus Tani's quartic. In terms of the normalized coordinate (Y/δ_i), the slope at the surface $a = (\delta_i/u_e)(\partial u/\partial Y)_0 = -4.887$ for the quartic profile (see Fig. 2b), whereas the slope of the lower branch solution approaches zero at the surface as $\beta \to 0$ (Fig. 2c). Actually, the lower branch solution approaches the Chapman[31] "free-mixing" profile as $\beta \to 0$ (Fig. 2d). In this limiting case, the outer shear-layer thickness is negligible compared to the thickness of the recirculating zone, i.e., $(Y/\delta_i)_{\psi=0} \to 1$, $(u/u_e)_{\psi=0} \to 0.587$, and the influence of the surface virtually disappears.

The compressible flow analog of the Falkner-Skan family was found by Cohen and Reshotko.[20] By assuming that $\mu \sim T$, $Pr = 1$, and $c_p = \text{const}$, and utilizing Stewartson's transformation,[32]

$$dX = (\rho_e a_e/\rho_\infty a_\infty)dx \qquad dY = (a_e\rho/a_\infty\rho_\infty)dy \tag{1}$$

they showed that the boundary-layer equations are transformed into an equivalent "low-speed" form, even when the flow is not adiabatic. The relation between the transformed and physical longitudinal velocity components is given by

$$U = (a_\infty/a_e)u \tag{2}$$

The equivalent Falkner-Skan family is generated by taking $U_e = CX^m$.

Numerical solutions of the boundary-layer equation for similar flow are tabulated by Cohen and Reshotko[20] for certain pairs of values of β and S_w, including a few "lower-branch" solutions; additional solutions can be obtained by numerical integration. For each value of S_w, the coupled velocity and total enthalpy profiles are determined completely by a single parameter, so that any convenient profile characteristic may be utilized in the two-moment scheme. For convenience, the profile parameter is selected as follows:

Attached Flow (upstream of separation and downstream of reattachment)

$$a(X) = \left[\frac{\partial(U/U_e)}{\partial(Y/\delta_i)}\right]_{Y=0} \tag{3}$$

where δ_i is the transformed boundary-layer thickness. In the present work,

$$0 \leqq a(X) \leqq 1.58 \text{ (Blasius)}$$

Separated Flow

$$a(X) = (Y/\delta_i)_{U=0} \qquad 0 \leqq a(X) \leqq 1 \tag{4}$$

i.e., $a(X)$ is the locus of the curve of zero velocity bounding the forward and reversed flow regions. All the required integral functions appearing in the two-moment equations for $a(X)$ and $\theta(X)$ [or $\delta_i^*(X)$] can be expressed in terms of $a(X)$ for a given value of S_w (Sec. 3.1).

At the cost of a certain amount of complication, the total enthalpy profiles can be specified independently of the velocity profiles, and the integral form of the energy equation can be added to the two velocity moment equations in order to determine the history of the additional parameter. For highly cooled flows, this procedure is essential, but for moderately cooled flows, we assume that the total enthalpy profile has no independent "memory." Of course this choice does not mean that the velocity and total enthalpy profiles are "similar" in the sense of the Crocco integral; in fact, the Cohen-Reshotko[20] solutions show that the total enthalpy profile is relatively insensitive to the velocity profile along the lower branch. At the separation and reattachment points, for example, the local surface heat-transfer rate does not vanish, even though the local skin friction is zero.§

§ See also Savage.[33]

3. Differential Equations and Properties of the Solutions

3.1 Differential Equations

By integrating the "reduced" momentum equation in Stewartson coordinates across the boundary layer, and making use of the continuity equation, one obtains[30, 33]

$$M_e(d\theta_i^2/dX) + 2[2 + (\delta_i^*/\theta_i) + (e/\theta_i)]\theta_i^2(dM_e/dX) = 2(\nu_\infty/a_\infty)(\theta_i/U_e)(\partial U/\partial Y)_{Y=0} \quad (5)$$

Similarly, by multiplying the momentum equation by U and integrating, one obtains[30, 33]¶

$$M_e\left(\frac{d\theta_i^{*2}}{dx}\right) + 2\left[3 + \left(\frac{2E}{\theta_i^*}\right)\right]\theta_i^{*2}\left(\frac{dM_e}{dx}\right) = 4\left(\frac{\nu_\infty}{a_\infty}\right)\left(\frac{\theta_i^*}{U_e^2}\right)\int_0^{\delta_i}\left(\frac{\partial U}{\partial Y}\right)^2 dY \quad (6)$$

where

$$\delta_i^* = \int_0^{\delta_i}\left[1 - \left(\frac{U}{U_e}\right)\right]dY \quad (7a)$$

$$\theta_i = \int_0^{\delta_i}\left(\frac{U}{U_e}\right)\left[1 - \left(\frac{U}{U_e}\right)\right]dY \quad (7b)$$

$$\theta_i^* = \int_0^{\delta_i}\left(\frac{U}{U_e}\right)\left[1 - \left(\frac{U^2}{U_e^2}\right)\right]dY \quad (7c)$$

$$e = \int_0^{\delta_i} S\,dY \quad (7d)^{**}$$

$$E = \int_0^{\delta_i}\left(\frac{U}{U_e}\right)S\,dY \quad (7e)^{**}$$

These equations are rewritten in the following more convenient form:

$$\mathfrak{C}(d\delta_t^*/dX) + \delta_t^*(d\mathfrak{C}/dX) + (2\mathfrak{C} + 1)\times(\delta_t^*/M_e)(dM_e/dX) = [\nu_\infty/(a_\infty M_e\delta_t^*)]P \quad (8)$$

$$J(d\delta_t^*/dX) + [\delta_t^*(dJ/d\mathfrak{C})](d\mathfrak{C}/dX) + (3J + 2S_wT^*)(\delta_t^*/M_e)(dM_e/dX) = [\nu_\infty/(a_\infty M_e\delta_t^*)]R \quad (9)$$

where††

$$\left.\begin{aligned} \delta_t^* &= \delta_i^* + e \\ \mathfrak{C} &= (\theta_i/\delta_t^*) \qquad J = (\theta_i^*/\delta_t^*) \\ R &= \left(\frac{2\delta_t^*}{U_e^2}\right)\int_0^{\delta_i}\left(\frac{\partial U}{\partial Y}\right)^2 dY \\ P &= (\delta_t^*/U_e)(\partial U/\partial Y)_{Y=0} \qquad T^* = (E/S_w\delta_t^*) \end{aligned}\right\} \quad (10)$$

In a viscous interaction of this type, the external inviscid flow is not known a priori, but is determined by the normal velocity induced by the growth of the boundary layer. As shown by Crocco and the senior author,[15] the inclination of the streamline in the external inviscid flow at $y = \delta$ is given by the relation

$$\tan\Theta = \left(\frac{v_e}{u_e}\right) = \left(\frac{d\delta^*}{dx}\right) - \left[\left(\frac{d}{dx}\right)(\log\rho_e u_e)\right]\int_0^{\delta}\left(\frac{\rho u}{\rho_e u_e}\right)dy \quad (11)$$

By applying the Stewartson transformation [Eq. (1)], Eq (11) becomes

$$(1/m_e)[(1 + m_e)/(1 + m_\infty)]\tan\Theta = \{[(1 + m_e)/m_e] + \mathfrak{C}\}d\delta_t^*/dX + \delta_t^*(d\mathfrak{C}/dX) + (f\delta_t^*/M_e)(dM_e/dX) \quad (12)$$

where

$$m = [(\gamma - 1)/2]M^2$$

$$f = 2\mathfrak{C} + [(3\gamma - 1)/(\gamma - 1)] + [(\gamma + 1)/(\gamma - 1)][m_e/(1 + m_e)]\mathfrak{C} + \{(M_e^2 - 1)/[m_e(1 + m_e)]\}Z$$

$$Z = (1/\delta_t^*)\int_0^{\delta_i}(U/U_e)dY$$

Usually, the compression waves generated by the growth of the boundary layer coalesce into a shock wave well beyond the outer edge of the layer (Fig. 1), so that the isentropic Prandtl-Meyer relation between M_e and Θ is a good approximation, i.e.,

$$\nu_{\infty\pm} - \nu(M_e) = \Theta \quad (13a)$$

where

$$\nu(M_e) = \left(\frac{\gamma + 1}{\gamma - 1}\right)^{1/2}\tan^{-1}\left\{\left(\frac{\gamma - 1}{\gamma + 1}\right)^{1/2}(M_e^2 - 1)^{1/2}\right\} - \tan^{-1}(M_e^2 - 1)^{1/2} \quad (13b)$$

$$\nu_{\infty\pm} = \nu(M_{\infty\pm}) \quad (13c)$$

and $M_{\infty-}$ is the Mach number far upstream of the interaction, and $M_{\infty+}$ is the Mach number far downstream of the interaction. If the supersonic-hypersonic similarity parameter $(M_e^2 - 1)^{1/2}\tan\Theta$ is small compared to unity, and $\tan\Theta \cong \Theta$, Eqs. (12a) and (13b) are replaced by the linearized Prandtl-Meyer relation:

$$\Theta = -\frac{(M_{\infty\pm}^2 - 1)^{1/2}}{(1 + m_{\infty\pm})}\left(\frac{\epsilon}{M_{\infty\pm}}\right) \quad (13d)$$

where

$$M_e = M_{\infty\pm} + \epsilon \quad (13e)$$

When Eqs. (12–13e) are combined with Eqs. (8) and (9), we have three simultaneous first-order nonlinear differential equations for the three dependent variables $M_e(X)$, $\delta_t^*(X)$, and $\mathfrak{C}(X)$, or $a(X)$.

As stated in Sec. 2.3, the quantities $\mathfrak{C}$, J, P, R, T^*, and Z appearing in Eqs. (8, 9, and 12) are to be evaluated as functions of $a(X)$ and S_w by utilizing the Cohen-Reshotko velocity and enthalpy profiles, including the analog of the Stewartson lower branch for separated and reattaching flow. We follow a procedure similar to that used by Thwaites[26] for the momentum equation and curve-fit‡‡ these functions in terms of the parameter a. For example, for adiabatic flow ($S_w = 0$), we have:

Attached Flow ($0 \leqslant a \leqslant 4$)

$$\mathfrak{C} = 0.2470 + 0.1095a - 0.0172a^2 + 0.00104a^3$$

$$J = 0.3737 + 0.1725a - 0.0199a^2 + 0.00070a^3$$

$$P = 0.4878a - 0.0963a^2 + 0.0077a^3$$

$$R = 1.2578 - 0.5259a + 0.2636a^2 - 0.0548a^3 + 0.00435a^4$$

$$Z = 1.0384 - 0.5894a - 0.0466a^2 + 0.0760a^3 - 0.0341a^4$$

¶ Alternatively, one could use the energy integral, or integral of the equation for the total enthalpy; this procedure is presently being studied.

** In Savage's notation,[33] $\xi \equiv e$ and $\mathcal{E} = E$.

†† Glick[15] showed that different choices of δ_i within reasonable bounds do not affect the final results in the Crocco-Lees mixing theory. A similar insensitivity is found with the present method.

‡‡ These functions are improved versions of those given in AIAA Preprint 64-4 and were found by John Klineberg of California Institute of Technology on the basis of further solutions of the Cohen and Reshotko equations.

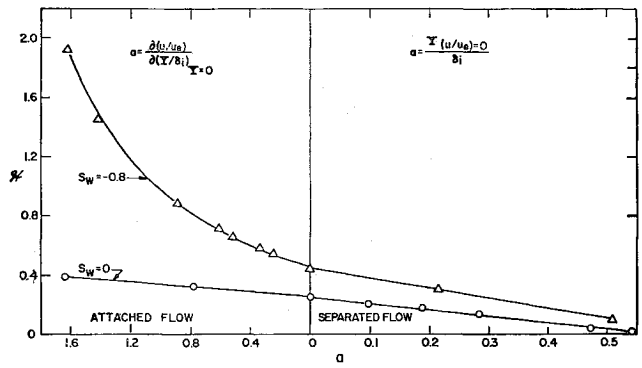

Fig. 3 Theoretical $\mathcal{H}$ distributions from similar solutions.

$$dJ/d\mathcal{H} = 1.575 + 0.0889a + 0.0595a^2 - 0.01059a^3$$

$$E = e \equiv 0$$

Separated ($0 \leqslant a \leqslant 0.54$)

$$\mathcal{H} = 0.2470 - 0.2589a + 0.0486a^2 - 3.721a^3 + 8.155a^4 - 4.586a^5$$

$$J = 0.3737 - 0.3788a - 0.2348a^4 - 2.883a^3 + 7.107a^4 - 4.087a^5$$

$$P = 2.001a - 11.40a^2 + 63.22a^3 - 75.04a^4 - 141.86a^5 + 321.77a^6 - 160.4a^7$$

$$R = 1.2578 - 0.5907a + 41.85a^2 + 256.2a^3 - 802.5a^4 - 1114.4a^5 + 581.8a^6$$

$$Z = 1.0384 - 0.5894a - 4.665a^2 + 7.598a^3 - 3.407a^4$$

$$dJ/d\mathcal{H} = 1.575 - 3.496a + 34.993a^2 - 187.9a^3 + 492.7a^4 - 671.96a^5 + 420.28a^6$$

These functions are shown in Figs. 3–8, along with the values computed directly from the similar solutions. The complete family of separated flow profiles extends over the range $0 < a < 1$, but the largest value of a for which a solution of the Falkner-Skan equations was obtained by Stewartson[19] is 0.54. By limiting the present analysis to values of $a < 0.54$, we are, in effect, placing an upper bound on the incident shock strength (or wedge angle for the flow past a wedge on a plate). Additional values for $0.54 < a < 1$ can of course be found by numerical integration if required.

As an illustration of the effect of heat transfer, consider the "highly cooled" case $S_w = -0.8$. For this case, Cohen and Reshotko[20] have found two lower branch solutions, in addition to an incipient separation solution, and several attached flow solutions as well. The functions $\mathcal{H}$, J, P, R, Z, and T^* were evaluated from the Cohen and Reshotko solutions, assuming that the dynamical and thermal boundary-layer thicknesses are equal§§ (Figs. 3–8).

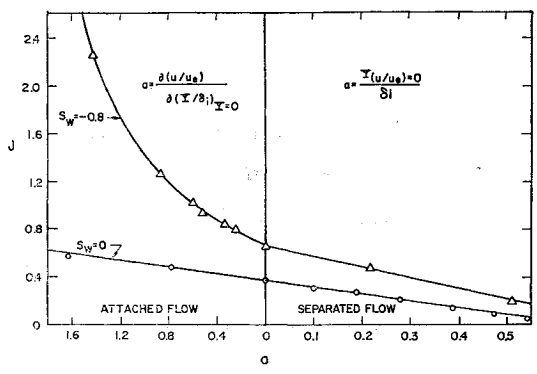

Fig. 4 Theoretical J distributions from similar solutions.

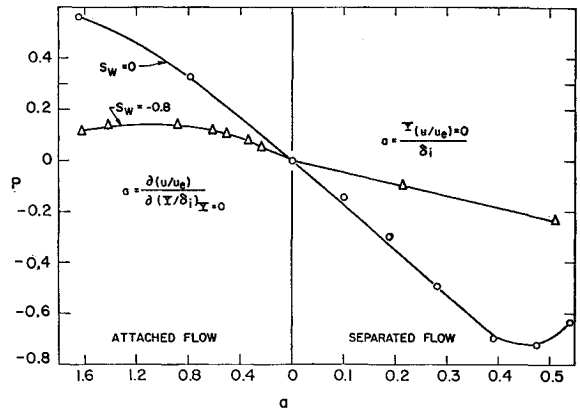

Fig. 5 Theoretical P distributions from similar solutions.

3.2 Subcritical and Supercritical Flows

In Sec. 2.1 we alluded briefly to the distinction between subcritical and supercritical laminar boundary-layer flows. Now we want to give a mathematical treatment of this question within the present theoretical framework and to offer a rough physical explanation of the different behavior of the flow in the two cases.

For convenience, the three governing differential equations (slightly rewritten) are repeated here [Eqs. (8, 9, and 12)]:

Continuity

$$B(d/dX)(\log\delta_t^*) + (d\mathcal{H}/dX) + f(d/dX)(\log M_e) = -[\nu_\infty/a_\infty M_e(\delta_t^*)^2]h \quad (14)$$

Momentum

$$\mathcal{H}(d/dX)(\log\delta_t^*) + (d\mathcal{H}/dX) + (2\mathcal{H} + 1)(d/dX)(\log M_e) = [\nu_\infty/a_\infty M_e(\delta_t^*)^2]P \quad (15)$$

First Moment of Momentum

$$J(d/dX)(\log\delta_t^*) + (dJ/d\mathcal{H})(d\mathcal{H}/dX) + (3J + 2S_wT^*)(d/dX)(\log M_e) = [\nu_\infty/a_\infty M_e(\delta_t^*)^2]_\infty R \quad (16)$$

where

$$B = \left[\mathcal{H} + \left(\frac{1 + m_e}{m_e}\right)\right] \qquad h = -\tilde{R}e_{\delta_t^*}\frac{(1 + m_e)}{m_e(1 + m_\infty)}\tan\Theta \quad (17)$$

When

$$(M_e^2 - 1)^{1/2}\tan\Theta \ll 1 \qquad \tan\Theta \equiv \Theta$$

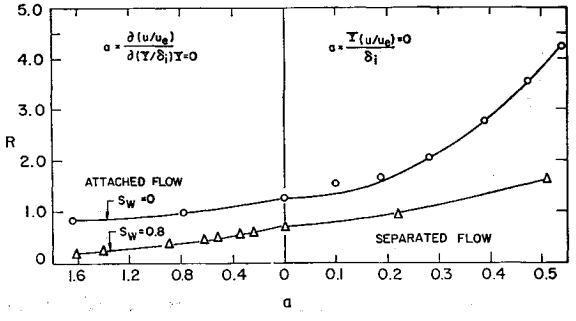

Fig. 6 Theoretical R distributions from similar solutions.

§§ Actually, for positive pressure gradients, $\delta_{\text{dynam}} > \delta_{\text{therm}}$. Cohen and Reshotko[20] have shown that, at the steepest gradients, near separation $(\delta_T/\delta_d) \cong 0.9$. Hence, this difference is clearly a second-order effect.

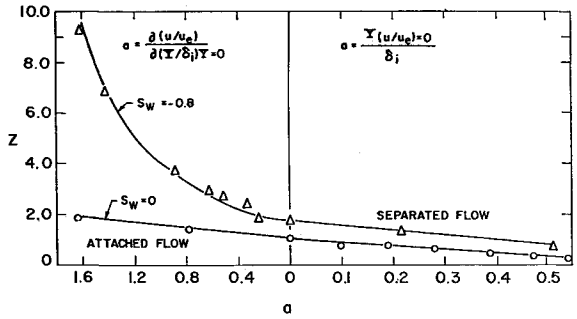

Fig. 7 Theoretical Z distributions from similar solutions.

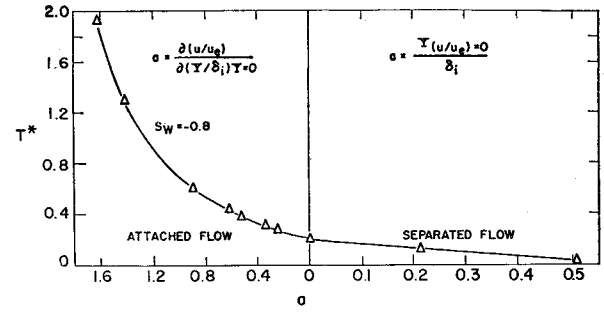

Fig. 8 Theoretical T^* distribution from similar solutions.

then [Eq. (13d)]

$$h = \tilde{R}e_{\delta t^*}\left(\frac{1+m_e}{m_e}\right)\frac{(M_{\infty\pm}^2-1)^{1/2}}{(1+m_\infty)(1+m_{\infty\pm})}\left(\frac{\epsilon}{M_{\infty\pm}}\right) \quad (17a)$$

By regarding these three equations as algebraic equations for $(d\delta_t^*/dX)$, $(d\mathfrak{IC}/dX)$, and (dM_e/dX), and solving simultaneously, one obtains

$$(\delta_t^*/M_e)(dM_e/dX) = (1/\tilde{R}e_{\delta t^*}) \times \{[N_1(\mathfrak{IC}, M_e, h)]/[D(\mathfrak{IC}, M_e)]\} \quad (18)$$

$$\delta_t^*(d\mathfrak{IC}/dX) = (1/\tilde{R}e_{\delta t^*})\{[N_2(\mathfrak{IC}, M_e, h)]/[D(\mathfrak{IC}, M_e)]\} \quad (19)$$

$$(d\delta_t^*/dX) = (1/\tilde{R}e_{\delta t^*})\{[N_3(\mathfrak{IC}, M_e, h)]/[D(\mathfrak{IC}, M_e)]\} \quad (20)$$

where

$$\tilde{R}e_{\delta t^*} = a_\infty M_e\, \delta_t^*/\nu_\infty \quad (21)$$

and

$$D(\mathfrak{IC}, M_e) = [(1+m_e)/m_e][(3J + 2S_wT^*) - (2\mathfrak{IC}+1)(dJ/d\mathfrak{IC})] + [(2\mathfrak{IC}+1) - f][J - \mathfrak{IC}(dJ/d\mathfrak{IC})] \quad (22a)$$

$$N_1(\mathfrak{IC}, M_e, h) = [(1+m_e)/m_e][R - P(dJ/d\mathfrak{IC})] + (P+h)[J - \mathfrak{IC}dJ/d\mathfrak{IC}] \quad (22b)$$

$$N_2(\mathfrak{IC}, M_e, h) = [(1+m_e)/m_e] \times [(3J + 2S_wT^*)P - R(2\mathfrak{IC}+1)] + (P+h)[\mathfrak{IC}(3J + 2S_wT^*) - fJ] + (R\mathfrak{IC} + Jh)[f - (2\mathfrak{IC}+1)] \quad (22c)$$

$$N_3(\mathfrak{IC}, M_e, h) = (P+h)[f(dJ/d\mathfrak{IC}) - (3J + 2S_wT^*)] - [f - (2\mathfrak{IC}+1)][R + h(dJ/d\mathfrak{IC})] \quad (22d)$$

Consider the possible "trajectories" of solutions of the boundary-layer/shock-wave interaction problem in the a-X and M_e-X planes in the region upstream of separation (Fig. 9). At the separation point ($a = 0$) one can show that $D < 0$ for all values of S_w and M_e. At this point, $P = 0$, so $N_1 > 0$ unless the Reynolds number is very high [Eqs. (17) and (22b)].¶¶ Similarly $N_2 > 0$ and $N_3 < 0$, or $(1/M_e)(dM_e/dX) < 0$, $(d\mathfrak{IC}/dX) < 0$, $(d\delta_t^*/dX) > 0$. Thus, the laminar boundary layer is subcritical at separation. This result is hardly surprising; one would not expect the boundary layer to separate from the surface unless $(1/M_e)(dM_e/dX) < 0$.

The integration of Eqs. (18–20) in the upstream direction proceeds smoothly from the separation point toward the flat-plate solution, as long as as $D \neq 0$ in the interval $0 \leqq a \leqq a_b$, i.e., as long as the flow remains subcritical [case 1, Fig. 9]. Now the location of the singular point defined by the condition $D = 0$ depends only on M_e and S_w and not on the Reynolds number [Eq. (22a)]. In Fig. 10a the value of $a = a_1$ for $D = 0$ is plotted as a function of Mach number for adiabatic flow ($S_w = 0$). In that case, the singularity always falls in the range $a > a_b$, corresponding to a boundary layer subjected to a sufficiently strong negative pressure gradient. Thus if the boundary layer "entering" the interaction zone is a self-preserving Blasius flow, the adiabatic interaction is always subcritical. However, when the flow is highly cooled and $M_e \gg 1$, the laminar boundary layer may go supercritical for $a < a_b$ because a large portion of the boundary layer is actually supersonic. In order to study this question more carefully, we propose to add the energy conservation integral to Eqs. (8, 9, and 12); the results of this study will be reported in Part II.

If, for example, the entering boundary layer is sufficiently "accelerated," so that $a_{-\infty} > a_1(M_e)$, then the singularity $D = 0$ does occur within the range $0 < a < a_{-\infty}$. This singular point corresponds to the "sonic point" in a nozzle. Unless N_1, N_2, and N_3 also vanish at this point, the "solution" is "turned back" and proceeds downstream along the supercritical branch (case 2, Fig. 9). These two branches are analogous to the two branches of the flow in the diverging or exit section of a nozzle.

This discussion shows that a supercritical laminar boundary layer cannot be joined smoothly to the flow near separation. A sudden "jump" must occur to the "subcritical branch" of the solution passing through separation (Fig. 11). The strength of this "jump" is determined by applying the appropriate "conservation" equations derived from Eqs. (14–16).* If the "final" laminar boundary layer downstream of the interaction region is subcritical, the flow downstream of the jump remains subcritical, but if the downstream

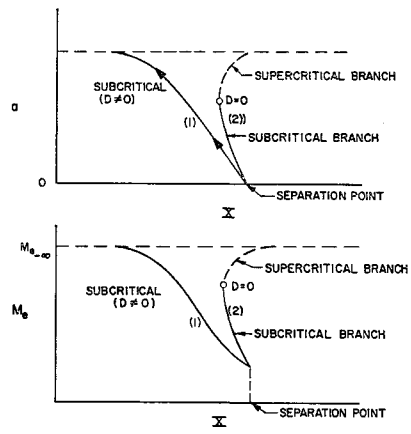

Fig. 9 Schematic representation of possible trajectories upstream of separation.

¶¶ At the separation point $J > \mathfrak{IC}(dJ/d\mathfrak{IC})$ and $\tan\Theta > 0$ or $[\epsilon < 0]$; thus, if $Re_{\delta_t^*}$ is high enough, the quantity h[(Eq. (17)] is a large enough negative number to outweigh the term $[(1+m_e)/m_e]$ R in Eq. (22b). However, this situation usually occurs beyond the range of interest for laminar flows, and it signals a breakdown of the one-parameter method when it does occur (Sec. 5).

* This problem is under investigation by John Klineberg at this laboratory, and the results will appear in Part II of this study.

laminar layer is also supercritical, the flow must pass through a "throat" downstream of shock impingement (Fig. 11). The location of the throat is given by the condition that N_1, N_2, N_3, and D vanish simultaneously; this throat, or saddle-point, is entirely analogous to the "critical point" found in the Crocco-Lees mixing theory for wake flows. Evidently, only one pair of conditions $D = 0$, $N_j = 0$ ($j = 1, 2$, or 3) is independent. If $N_1 = 0$, for example [Eq. (22b)],

$$h = \left[\frac{(1 + m_e)}{m_e}\right]\left[\frac{P(dJ/d\mathfrak{IC}) - R}{J - \mathfrak{IC}(dJ/d\mathfrak{IC})}\right] - P \qquad (23)$$

By substituting the values of a_1 and M_e for $D = 0$ into Eq. (23), one finds that $\Theta > 0 (\epsilon < 0)$ at the throat (Fig. 10b). The actual location of the throat is given by Eq. (23) and the relation $a = a_1(M_e)$. Thus, in many respects laminar boundary-layer/shock-wave interaction with an initially supercritical flow is similar to adiabatic turbulent boundary-layer interaction.

Whether one is dealing with an "accelerated" adiabatic laminar boundary layer ($a > a_b$), or with a highly cooled flat-plate layer, the supercritical character of the flow is caused by the behavior of the displacement thickness δ_t^*. In these flows, the mass flux across the layer is relatively high, so that $\delta_t^*/\delta_i \ll 1$. However, even a small reduction in negative pressure gradient (if $a > a_b$), or a small positive pressure gradient if $a = a_b$, produces a rapid increase in (δ_t^*/δ_i) in the downstream direction as a increases. Now

$$(d\delta_t^*/dX) = (\delta_t^*/\delta_i)(d\delta_i/dX) + \delta_i(d/dX)(\delta_t^*/\delta_i)$$

and $(d\delta_t^*/dX)$ is small if Θ is small, according to Eq. (15). But $(d/dX)(\delta_t^*/\delta_i)$ is so large that $(d\delta_i/dX) < 0$! In other words, $(d\delta_i/dp) < 0$; this situation is characteristic of supercritical flows such as the steady supersonic flow in a nozzle

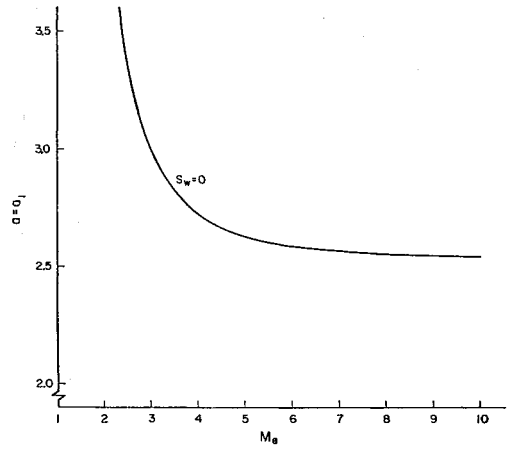

Fig. 10a Location of singular point, $D = 0$, as a function of Mach number.

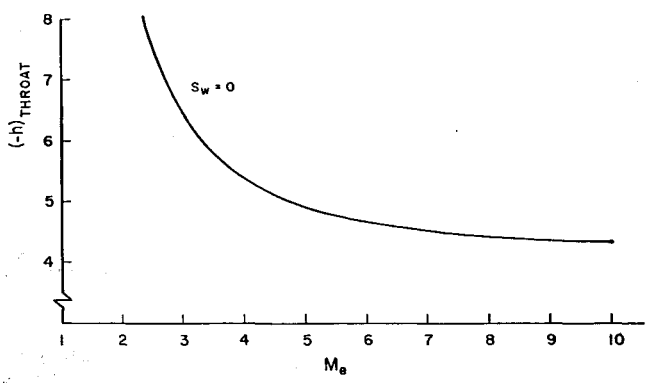

Fig. 10b Variation of h_{throat} with Mach number.

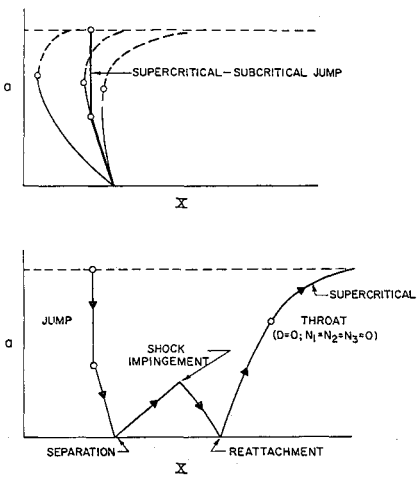

Fig. 11 Schematic representation of supercritical laminar boundary-layer/shock-wave interaction.

where $(dA/dp) < 0$. Thus it is not surprising that small disturbances cannot propagate upstream in a supercritical flow.

According to the momentum equation [Eq. (6) or (18)], θ_i increases gradually if $(dp/dX) > 0$. We know that (θ_i/δ_i) is slowly varying with a, so momentum considerations require that $(d\delta_i/dp) > 0$, in contradiction to the condition imposed by continuity. Thus, we conclude that a smooth compression is impossible in a supercritical flow. On the other hand, an expansion offers no difficulty because (δ_t^*/δ_i) decreases as a increases.

3.3 Nature of Solutions for Subcritical Laminar Boundary-Layer/Shock-Wave Interaction

3.3.1 Upstream of separation

The interaction between the laminar boundary layer and the external supersonic flow upstream of separation is completely determined by the Reynolds number and the previous history of the boundary layer. In the present study, the boundary layer "entering" the interaction zone is a self-preserving Blasius flow, so the derivatives $(dM_e/d\delta_t^*)$ and $(da/d\delta_t^*)$ must both vanish as $a \to a_b$ along the integral curve from the separation point. Thus N_1, $N_2 \to 0$ according to Eqs. (18) and (19), but $N_3 \neq 0$, $D \neq 0$ as $a \to a_b$. These conditions are satisfied only if

$$\mathfrak{IC}R = PJ \qquad (24)$$

and [Eqs. (17a, 23, and 24)]

$$\epsilon = -\left(\frac{P_b}{\mathfrak{IC}_b}\right)\left\{\left[\frac{(1 + m_{\infty-})}{(m_{\infty-})}\right] + \mathfrak{IC}_b\right\} \times \left[\frac{(m_{\infty-})(1 + m_\infty)}{(M_{\infty-}^2 - 1)^{1/2}}\right]\left[\frac{\nu_\infty}{(a_\infty \delta_t^*)}\right] \qquad (25)$$

and, if $M_\infty \gg 1$,

$$\epsilon \cong -(1 + \mathfrak{IC}_b)(P_b/\mathfrak{IC}_b)[\nu_\infty/(a_\infty \delta_t^*)](m_\infty^2/M_{\infty-}) \qquad (25a)$$

The first relation determines the value of a corresponding to the Blasius profile ($a_b = 1.58$, all S_w and M_e), whereas Eq. (25) or (25a) yields the well-known[3] induced pressure distribution for "weak interaction."†

For convenience in numerical integration, Eqs. (18–20) are rewritten in the form

$$(\delta_t^*/M_e)(dM_e/d\delta_t^*) = (N_1/N_3) \qquad (26)$$

$$\delta_t^*(da/d\delta_t^*) = (N_2/N_3)[1/(d\mathfrak{IC}/da)] \qquad (27)$$

† The basic equations [(18–20)] also yield the hypersonic "strong" interaction solution upstream of the interaction zone when $[M_\infty^3/(Re_{x_0})^{1/2}] \gg 1$.

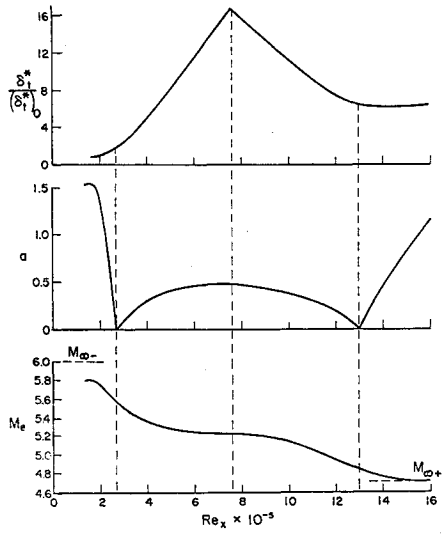

Fig. 12 δ_t^*, a, and M_e trajectories for a shock-wave/boundary-layer interaction at $M_\infty = 6$, $S_w = 0$ (adiabatic flow).

A value of $\Theta = \Theta_s$ [or $\epsilon = \epsilon_s$] is specified at the separation point ($a = 0$) and a trial value of $\delta_{t_s}^*$ selected. Integration of Eqs. (26) and (27) was performed using a Runge-Kutta technique on an IBM 7090 digital computer. By iteration, the correct value of $\delta_{t_s}^*$ and the proper integral curve are determined as the solution of a typical two-point boundary-value problem, in which N_1 and N_2 must vanish simultaneously upstream as $a \to a_b$. The point at which $N_1 = N_2 = 0$ and $a = a_b$ is defined as the beginning of the interaction, and the value of δ_t^* at this point fixes the "initial" Reynolds number. Typical $a(M_e)$ and $\delta_t^*(M_e)$ trajectories for an adiabatic laminar boundary-layer/shock-wave interaction on a flat plate are shown in Fig. 12.

Upstream of separation $(d\delta_t^*/dM_e) < 0$, $(da/d\delta_t^*) < 0$, and $(da/dM_e) > 0$. By proper choice of ϵ or h at $a = a_b$, the signs of N_1 and N_2 can be changed, so that $(da/dM_e) > 0$, but $(d\delta_t^*/dM_e) > 0$ and $(da/d\delta_t^*) > 0$. This branch represents the interaction of an expansion fan with a laminar boundary layer, in which $a > a_b$ in the interaction zone. Clearly, other "initial" conditions corresponding to the effect of surface curvature can also be analyzed by this method.

Once Eqs. (26) and (27) are solved, the results are transformed back to the physical plane by means of the integral

$$\int_{x_0}^{x} dx = \int_{\delta_{t_0}^*}^{\delta_t^*} \left[\frac{(1+m_e)}{(1+m_\infty)}\right]^{(3\gamma-1)/[2(\gamma-1)]} x\left(\frac{a_\infty}{\nu_\infty}\right)\left(\frac{M_e\delta_t^*}{R}\right) \times \left[\delta_t\left(\frac{d\mathfrak{K}}{da}\right)\left(\frac{dJ}{d\mathfrak{K}}\right)\left(\frac{da}{d\delta_t^*}\right) + J + (3J + 2S_wT^*)\left(\frac{\delta_t^*}{M_e}\right)\left(\frac{dM_e}{d\delta_t^*}\right)\right] d\delta_t^* \quad (28)$$

3.3.2 *Region between separation and shock impingement*

Between separation and reattachment, $a = (Y/\delta_i)_{U=0}$. According to Eq. (19), (da/dX) is always positive (and finite) at the separation point. Thus the locus of zero velocity breaks away from the separation point at a finite angle to the surface. The Stewartson lower branch solutions have the property that $[(d/da)(Y/\delta_i)_{\psi=0}]_{a\to 0} = \text{const}$ (1.5); hence, the dividing streamline also separates from the surface at a finite angle. The present results correspond to the local regular solution around the separation point found by Oswatitsch.[23] Similar remarks apply to the reattachment point.

The solution of Eqs. (26) and (27) downstream of the separation point is uniquely determined by the conditions at separation; namely, $a = 0$, $\delta_t^* = (\delta_t^*)_s$, $\Theta = \Theta_s$, already found from the upstream solution (Sec. 3.3.1). The integral curves show that a increases steadily with X (Fig. 12); the upper bound $a = 1$ corresponds to the Chapman[31] mixing profile. This portion of the integral curve may be terminated at any value of a (or X) at which one wishes to place the incident oblique shock. Of course, the larger the value of a the stronger will be the corresponding incident shock and the more extensive the upstream interaction region (Sec. 4) ‡

3.3.3 *Downstream of shock impingement: reattachment*

As discussed in Sec. 2.1, the local "external" Mach number M_e is continuous at the shock impingement point, or

$$\Theta_2 = \nu_{\infty+} + \Theta_1 - \nu_{\infty-}$$

In the linearized case,

$$\epsilon_2 = M_{\infty-} + \epsilon_1 - M_{\infty+}$$

where the subscripts 1 and 2 refer to conditions just upstream and downstream of the shock. Since a is also continuous, its value is known, and either $M_{\infty+}$ or Θ_2 (or ϵ_2) is utilized as an iteration parameter for the downstream integration. The correct integral curve is determined by the condition $N_1, N_2 \to 0$ as $a \to a_b$ and $M_\infty \to M_{\infty+}$.

Downstream of shock impingement, all three quantities a, M_e, and δ_t^* decrease to the reattachment point (Fig. 12). Downstream of reattachment

$$a = \{\partial(U/U_e)/[\partial(Y/\delta_i)]\}_{Y=0}$$

and $(da/dX) > 0$. At some point downstream of reattachment $N_3 = 0$ and $(d\delta_t^*/dX) = 0$ (but $\Theta \neq 0$ there !); the flow passes through a "neck" in the $\delta_t^* - X$ plane and $(d\delta_t^*/dX) > 0$ beyond this point. Near reattachment $(dM_e/dX) < 0$, so $(dM_e/da) < 0$. But we know that $(dM_e/da) > 0$ in the vicinity of the flat-plate solution (Sec. 3.3.1), so the Mach number must undershoot and the static pressure must overshoot slightly before the final equilibrium flow is achieved (Fig. 12).

4. Laminar Boundary-Layer/Shock-Wave Interaction for Adiabatic Flow

4.1 Interaction Upstream of Disturbance

As we have seen, the Tani[18] quartic is a poor representation of velocity profiles in flows with extensive separation (Sec. 2.3). As an illustration of this fact, Fig. 13 shows theoretical static pressure distributions, computed with both similar solution and quartic profiles, for flow upstream of a disturbance which is sufficiently strong to separate the boundary layer. As one might expect, upstream of separation the two

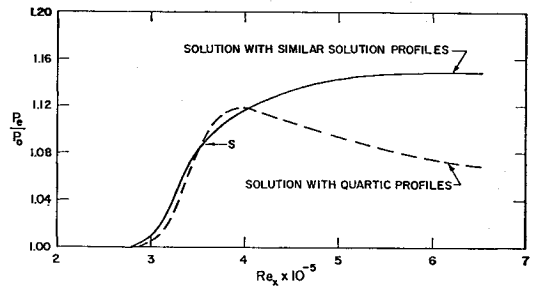

Fig. 13 Comparison of theoretical pressure distributions upstream of a disturbance.

‡ In other words, this scheme is an "inverse" method. Comparison with experimental measurements is made by selecting several different locations of the shock impingement point bracketing the location used in the experiments (see Fig. 20, for example). We wish to re-emphasize here that there are no semiempirical factors introduced into the calculation.

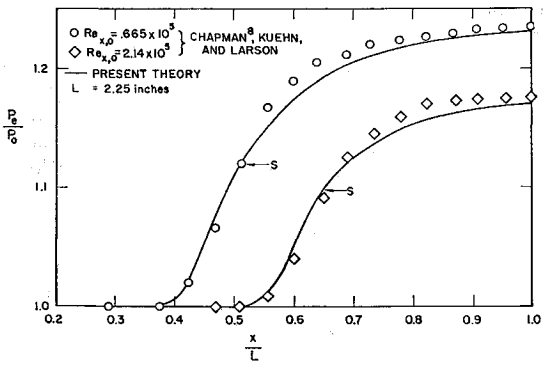

Fig. 14 Experimental and theoretical pressure distributions upstream of a disturbance at $M_\infty = 2$.

solutions are in very good agreement. Downstream of separation the quartic solution exhibits a maximum in static pressure followed by a region of negative pressure gradient. The solution with similar solution profiles, on the other hand, shows a monotonically decreasing positive pressure gradient and an eventual plateau. This plateau in static pressure has been observed experimentally and apparently is crucial in providing just the right amount of mixing between the inviscid flow and separated shear layer so that the layer can ultimately reattach.

Figure 14 shows a comparison of theoretical and experimental[8] pressure distributions upstream of a disturbance for different Reynolds numbers at Mach 2. The data shown were obtained for flow past a wedge in contact with a flat plate. Both theory and experiment show that as Reynolds number is lowered the separation point moves upstream and the pressure ratios at separation and in the plateau are increased. The theoretical distributions of static pressure are in good agreement with the experimental results, although downstream of separation the theoretical distributions level off somewhat more rapidly.

Figure 15 shows a comparison of theoretical and experimental pressure distribution upstream of a disturbance in hypersonic flow. The data of Sterrett and Emery[22] correspond to the flow past a forward facing step in contact with a flat plate. At this Mach number, the theoretical plateau pressure is about 15% higher than the experimental value. The pressure at separation is in almost exact agreement with the experimental value.

4.2 Pressure Rise at Reattachment

The Chapman[8] theory of reattachment assumes that total pressure is conserved along the dividing streamline in the reattachment zone. As a consequence of this assumption, the reattachment pressure rise is completely determined by the local Mach number and the value of $u^* = (u/u_e)_{\psi=0}$ approaching the reattachment zone. According to this theory, the reattachment process itself is independent of Reynolds number, although for free interactions the value of u^* at

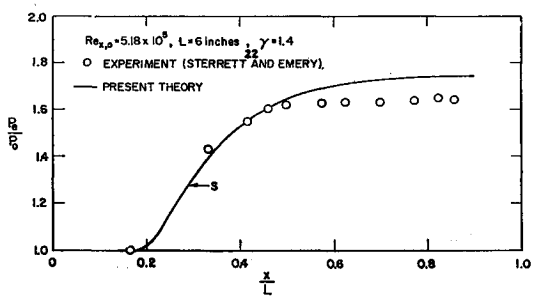

Fig. 15 Experimental and theoretical pressure distributions upstream of a disturbance at $M_\infty = 6.5$.

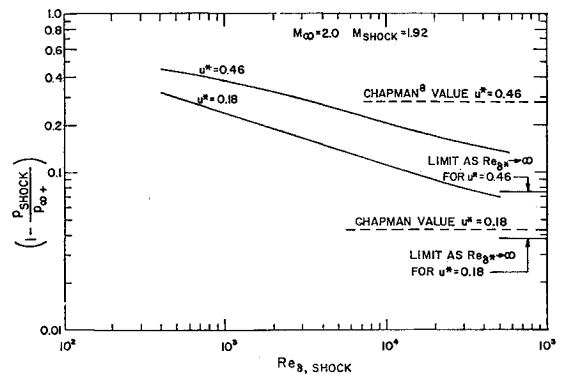

Fig. 16 Effect of Reynolds number on reattachment pressure ratio.

the beginning of reattachment may be Reynolds number dependent because the location of the separation point is not fixed. If we write the boundary-layer momentum equation along the dividing streamline

$$\rho u(du/dx) = -(dp/dx) + (\partial\tau/\partial y)_{\psi=0} \qquad (29)$$

we see that the assumption of constant total pressure is valid only when the normal gradient of shear at the dividing streamline is much less than the pressure gradient along the surface. The Stewartson lower branch velocity profiles have the property that $(\partial\tau/\partial y)_{\psi=0} > 0$; hence, it is apparent from Eq. (29) that deceleration along the dividing streamline is retarded by the shear gradient, and as a result the reattachment zone is lengthened. To put it another way, the static pressure rise for a given initial u^* is increased by the action of the viscous shear stress.

As the reattachment zone becomes relatively large, one can expect that shear and mixing with the outer inviscid flow will have an important role in determining the pressure rise, and the mechanism of reattachment will indeed be dependent upon Reynolds number. Figure 16 shows the theoretical variation of reattachment pressure ratio with Reynolds number. For given Mach number and constant u^*, the ratio $(p_{\infty+}/p_{\text{shock}})$ increases with decreasing Reynolds number and pressure coefficient varies approximately as

$$C_{PR} = \frac{1 - (p_{\text{shock}}/p_{\infty+})}{\frac{1}{2}\gamma M^2_{\text{shock}}} \sim \begin{cases} (Re_\delta^*)^{-1/4} & u^* = 0.46 \\ (Re_\delta^*)^{-1/3} & u^* = 0.18 \end{cases}$$

for

$$5 \times 10^2 < Re_\delta{}^*_{\text{shock}} < 5 \times 10^3$$

Hence, the effect of Reynolds number becomes less important as u^* is increased. As $Re_\delta^* \to \infty$, the pressure ratio approaches a constant depending on the value of u^*. As $Re_\delta^* \to \infty, h \gg 1$ [Eqs. (17–21)],

$$\left(\frac{M_e}{M_{e\text{shock}}}\right) = \exp\int_{a_{\text{shock}}}^{a}\left[\frac{J - \mathcal{K}(dJ/d\mathcal{K})}{J(\mathcal{K}-1) + 2S_wT^*\mathcal{K}}\right]\left(\frac{d\mathcal{K}}{da}\right)da$$

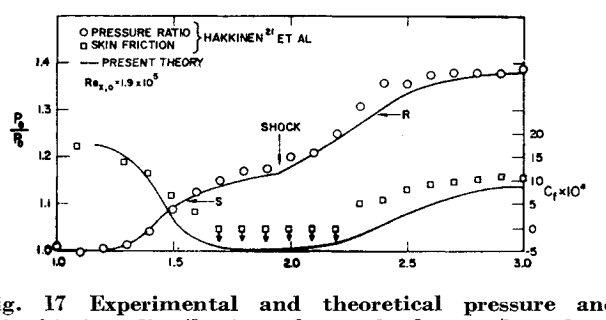

Fig. 17 Experimental and theoretical pressure and skin-friction distributions for a shock-wave/boundary-layer interaction at $M = 2.0$.

and we see that the reattachment pressure rise depends only upon a_{shock} and S_w. Also, the maximum pressure in the pressure overshoot downstream of the reattachment point occurs when $J - \mathcal{K}(dJ/d\mathcal{K}) = 0$ or a (attached) = 0.4 for adiabatic flow.

The limit $Re_\delta^* \to \infty$, $h \gg 1$ implies that P, $R \approx 0$, i.e., that shear at the wall and viscous dissipation become negligible. Furthermore, the momentum integral and first moment become uncoupled from the continuity integral [Eq. (11)], with the result that mixing also becomes unimportant in determining the reattachment pressure rise. Thus it is this limiting value of the pressure ratio as $Re_\delta^* \to \infty$ (Fig. 16) which corresponds conceptually to the Chapman model. Of course the value of the pressure rise obtained with the moment method differs from the Chapman value, because in the moment method the entire viscous layer is compressed isentropically.

4.3 Complete Interactions

Figures 17 and 18 show comparisons of the present theory with experimental pressure distributions[8, 21] in shock-wave boundary-layer interactions. In both cases, the pressure distributions up to the shock impingement point are in good agreement with experiment. In the reattachment region agreement is also quite good, although the theoretical pressure rises somewhat more slowly than in experiments. On the other hand, the calculated skin-friction coefficient seems to drop somewhat more rapidly than the experimental values upstream of separation and to rise more slowly downstream of reattachment.

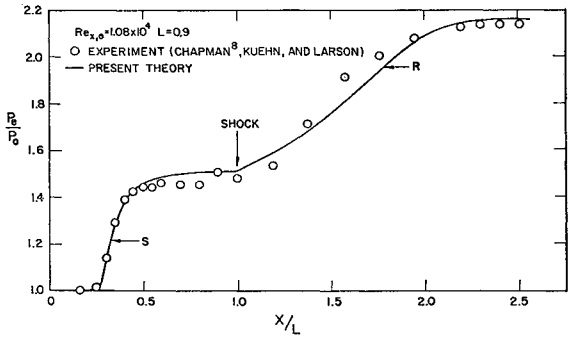

Fig. 18 Experimental and theoretical pressure distributions for a shock-wave/boundary-layer interaction at $M_\infty = 2.45$.

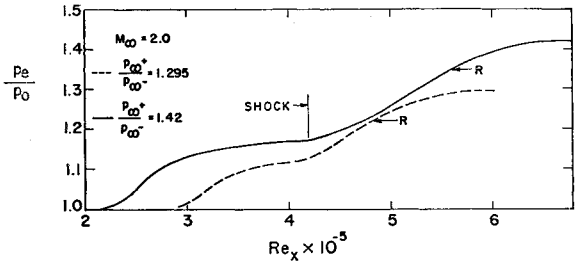

Fig. 19 Effect of shock strength on pressure distribution, $M_\infty = 2.0$.

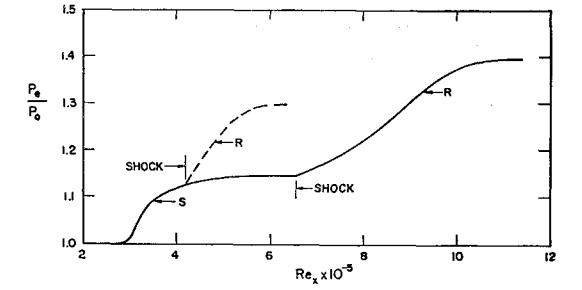

Fig. 20 Effect of varying shock strength and location for fixed separation point, $M_\infty = 2.0$.

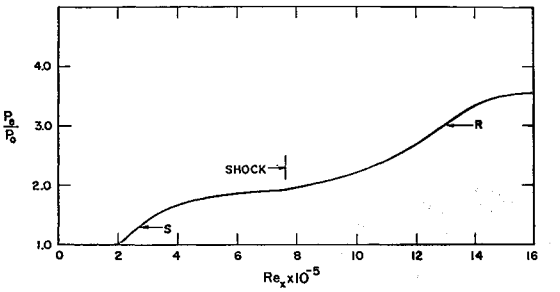

Fig. 21 Shock-wave/boundary-layer interaction at $M_\infty = 6$: pressure distribution.

Figure 19 shows the effect of shock strength on the static pressure distribution when the shock impingement point is fixed. As the shock strength increases, the separation point moves upstream, and both the separation and plateau pressures are increased. The reattachment point moves downstream with increasing shock strength, and hence the overall length of interaction is increased.

Figure 20 shows that, in order to keep the separation point fixed, the shock impingement point must move downstream as shock strength is increased. Apparently the location of shock impingement is rather sensitive to shock strength as long as the flow is laminar.

Figures 21 and 22 show the theoretical static pressure and displacement thickness distributions, respectively, for an interaction at Mach 6. In the separated region upstream of the shock the displacement thickness increases almost linearly to a factor of 7 greater than the displacement thickness at the beginning of the interaction. Apparently, for extensive separation, this thickness variation has a dominant effect on the skin-friction coefficient, as shown in Fig. 22. The shearing stress actually increases downstream of separation, after passing through a minimum, because of the rapidly thickening region of reverse flow. A similar effect is produced in the reattachment region as the thickness of the layer rapidly decreases.

5. Limitations of Two-Moment Method Based on One-Parameter Family of Velocity Profiles

In one of the examples of adiabatic boundary-layer/shock-wave interaction discussed in Sec. 4.1, the two-moment method based on the Tani[18] quartic velocity profile led to a static pressure maximum on the plate surface between separation and shock impingement (Fig. 13). On the other hand, calculations based on the Stewartson[19] family gave

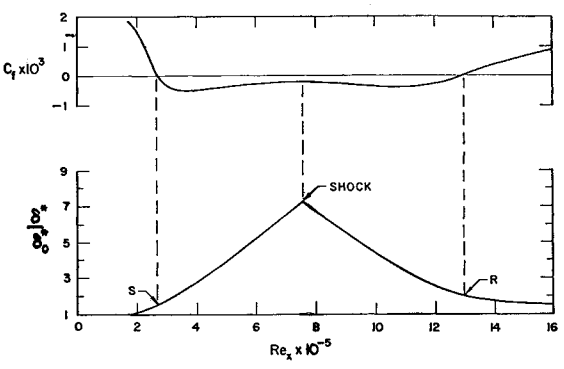

Fig. 22 Shock-wave/boundary-layer interaction at $M_\infty = 6$: skin-friction and displacement thickness distributions.

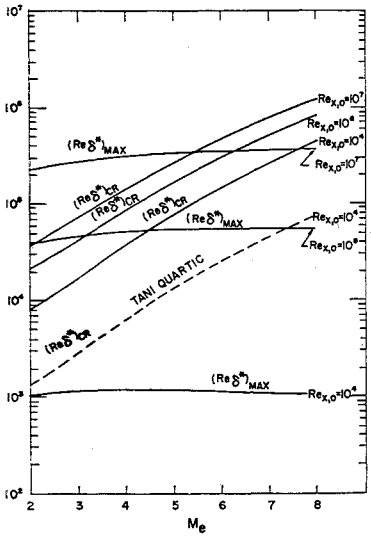

Fig. 23a Limitations on two-moment method based on Stewartson family: $S_w = 0$ (adiabatic flow).

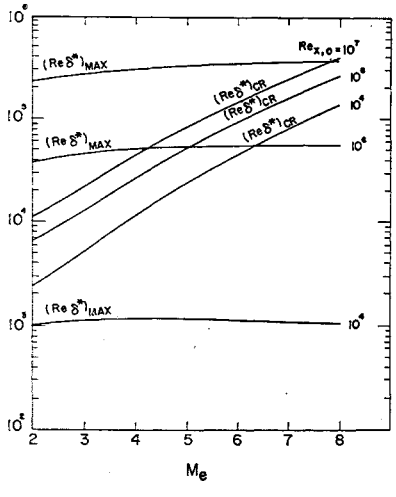

Fig. 23b Limitations on two-moment method based on Stewartson family: $S_w = -0.4$.

excellent agreement with the experimentally observed pressure plateau in all cases (Figs. 13–15, 17, and 18). The question naturally arises as to whether the Stewartson family, or indeed any other one-parameter family, could also lead to a physically unrealistic static pressure maximum for certain ranges of Mach number, Reynolds number, and enthalpy ratio S_w. The conditions under which such a pressure maximum first appears define the limits of applicability of the two-moment method based on a one-parameter family of velocity profiles.

According to Eq. (18), the conditions for the occurrence of a pressure maximum are that $N_1 = 0$ and $D \neq 0$; the first of these conditions leads to the relation already given by Eq. (23), i.e.,

$$h = -\tilde{R}e_{\delta t}^*[(1 + m_e)/m_e(1 + m_\infty)] \tan\Theta = [(1 + m_e)/m_e]\{[P(dJ/d\mathfrak{IC}) - R]/[J - \mathfrak{IC}(dJ/d)\mathfrak{IC}]\} - P \quad (23')$$

Since $R > P(dJ/d\mathfrak{IC})$, and the first term on the right-hand side is much larger than $(-P)$, a static pressure maximum can occur if $J > \mathfrak{IC}(dJ/d\mathfrak{IC})$, provided that $\tilde{R}e_{\delta t^*}$ is large enough so that Eq. (23) is satisfied at some point.

For the Stewartson family, $J \geq \mathfrak{IC}(dJ/d\mathfrak{IC})$ when $0 < a < 0.4$ upstream of separation and for all values of a between separation and shock impingement.§ Since the quantity $[J - \mathfrak{IC}(dJ/d\mathfrak{IC})]$ increases steadily with increasing $a = (Y/\delta_i)_{U=0}$ downstream of separation, the most stringent limitation on the value of h or $Re_{\delta t^*}$ is imposed by taking $a = 1$; here we relax this limitation somewhat by taking $a = 0.54$, corresponding to the upper limit of the tabulated Stewartson functions. Values of the function

$$G = [P(dJ/d\mathfrak{IC}) - R]/[J - \mathfrak{IC}(dJ/d\mathfrak{IC})]$$

for $a = 0.54$ computed from the Cohen-Reshotko[20] solutions are shown in Table 1.

In order to estimate the "critical" value of $Re_\delta^* = (Re_\delta^*)_{cr}$ at which a static pressure maximum first appears, we need to estimate the value of Θ at this point [Eq. (23)]. For this purpose we use the semiempirical equation for the plateau pressure coefficient given by Chapman et al.,[8]

$$C_p = C(M_\infty^2 - 1)^{-1/4}(Re_{x,0})^{-1/4} \quad (30)$$

where $C = 2$ for adiabatic flow; furthermore, we assume that the value of C is not changed much by heat transfer. By utilizing the well-known isentropic flow relations and Eq. (30), the Mach number corresponding to the plateau pressure can be computed as a function of M_∞ and $Re_{x,0}$. The estimated value of $\Theta_{plateau}$ is obtained from the Prandtl-Meyer relation

$$\nu_{-\infty} - \nu(M_e) = \Theta_{plateau} \text{ [Eq. (13a)]}$$

Finally, the value of $(Re_\delta^*)_{cr}$ is obtained from $(Re_{\delta t^*})_{cr}$ by using the defining relation

$$\delta^* = \delta_t^*[(1 + m_e)/(1 + m_\infty)]^{(\gamma+1)/[2(\gamma-1)]} \times [1 + m_e) + m_e\mathfrak{IC}] \quad (31)$$

In Figures 23a and 23b, $(Re_\delta^*)_{cr}$ is plotted as a function of M_∞ for values of $Re_{x,0}$ of 10^4, 10^6, and 10^7. For comparison, the value of $(Re_\delta^*)_{cr}$ corresponding to the Tani quartic is shown in Fig. 23a for adiabatic flow, with $Re_{x_0} = 10^4$; these values are almost one order of magnitude lower than those obtained using the Stewartson lower branch solutions. The difficulties encountered by Abbott, Holt, and Nielsen[12] are perfectly understandable on the basis of Fig. 23a.

These estimated values of $(Re_\delta^*)_{cr}$ must now be compared with the maximum values of Re_δ^* expected at the location of the static pressure maximum. A rough estimate of $(Re_\delta^*)_{max}$ is obtained by assuming that $(d\delta^*/dx) = \Theta_{PL}$ (const) where $\Theta_{PL} = \Theta_{plateau}$, or

$$(Re_{\delta^*})_{max} \cong [(x_m - x_s)/x_s]\Theta_{PL}\, Re_{x_s} \quad (32)$$

where x_m is the location of the pressure maximum. For our present purposes, it is sufficiently accurate to take $[(x_m - x_s)/x_s] = 1$ and $Re_{x_s} \cong Re_{x,0}$. Estimated values of $(Re_\delta^*)_{max}$ are shown in Figs. 23a and 23b for $Re_{x_0} = 10^4$, 10^6, and 10^7.

For fixed values of M_e and S_w, $(Re_\delta^*)_{cr} \sim Re_{x0}^{1/4}$ and $(Re_\delta^*)_{max} \sim Re_{x_0}^{3/4}$, roughly,[7, 8] so that any one-parameter family will always lead to an unrealistic static pressure maximum at sufficiently high values of Re_{x_0}. Of course when $Re_{x_0} > 10^6 - 10^7$, the boundary-layer flow is likely to be turbulent because the separated laminar flow velocity profiles are notoriously unstable to small disturbances, even for highly cooled surfaces. Nevertheless, it is instructive to consider the limiting case $Re_{x_0} \to \infty$ because it suggests the proper procedure for postponing the appearance of the pressure maximum, if necessary.

In the limit $Re_{x_0} \to \infty$, Eq. (18) shows that

$$(\delta_t^*/M_e)(dM_e/dX) \to -\{[J - \mathfrak{IC}(dJ/d\mathfrak{IC})]/D\} \times \{(1 + m_e)/[m_e(1 + m_e)]\} \tan\Theta \quad (33)$$

Now the Pohlhausen parameter is defined by

$$\Lambda = (\delta_t^{*2}/\nu_\infty)(dU_e/dX) = Re_{\delta t}^*[(\delta_t^*/M_e)(dM_e/dX)]$$

thus, $\Lambda \sim Re_x^{1/4}$ as $Re_{x_0} \to \infty$ [Refs. 7 and 8 and Eqs. (30) and (33)]. This physically unrealistic and mathematically

§ For Savage's velocity profiles,[33] $J \geq \mathfrak{IC}(dJ/d\mathfrak{IC})$ when $0 \leqq a \leqq 0.35$.

Table 1

S_w	G (similar solution, lower branch)	G (quartic)
0	−248	−43
−0.4	− 77.8	
−0.8	− 30.7	

untenable situation can be eliminated by employing a two-parameter, two-moment method such as Wieghardt's[29] in which $a(X)$ and $\Lambda(X)$ are the independent parameters. The condition of finiteness on Λ then insures that $(\delta_i^*/M_e) \times (dM_e/dX) \to 0$ properly as $Re_{x0} \to \infty$. Recently Makofski[34] utilized Wieghardt's[29] method for adiabatic flows. It would be interesting to apply this method to a highly cooled boundary layer at low supersonic Mach numbers and high Reynolds numbers.

6. Future Work

6.1 Effect of Heat Transfer

According to Eqs. (18–20), the length scale for the viscous-inviscid interaction along the plate surface is proportional to δ_i^*. At high Mach numbers, one sees from Eq. (31) and Fig. 3 that the value of $Re_{\delta i^*}$ for a given value of Re_δ^* is roughly one-half as large for a highly cooled boundary layer ($S_w = -0.8$) as it is for an adiabatic boundary layer. But for a given value of Re_{x_0},

$$(Re_\delta^*)_{S_w=-0.8}/(Re^*)_{S_w=0} \cong \tfrac{1}{4}$$

so the length scale is reduced by almost one order of magnitude if one considers only the effect of heat transfer on δ_i^*. This effect is certainly in the direction indicated by the few experimental results available.[35–37] Detailed calculations are now in progress and will be contained in Part II. It will also be interesting to compute the pressure jump across the initial "shock" in highly cooled supercritical flows as a function of enthalpy ratio and Mach number.

6.2 Base Flows and Wake Flows

Unless the Reynolds number is very low, the free shear layers shed from the aft portion of a blunt body at supersonic speeds are thin compared to the body radius. Initially these shear layers are directed toward the plane of symmetry. In two-dimensional flow they remain very nearly straight and the static pressure is constant for a certain distance. Then the flow begins to turn back toward the freestream direction, the static pressure begins to rise, and the two shear layers coalesce at the "neck." The fluid below the dividing streamline is returned to the recirculating flow just behind the base, whereas the fluid above this streamline flows downstream to form the "wake" proper.

Viscous-inviscid interactions of this type are contained within the framework of the general theory formulated in Sec. 3. However, one must replace the Stewartson[19] reversed-flow velocity profiles for flow over a solid surface by another family of solutions of the Falkner-Skan equation also found by Stewartson[19]; this family corresponds to viscous flows in a positive pressure gradient with zero shear on the axis, i.e., $f(0) = f''(0) = 0$. Again we "unhook" the profiles from the Falkner-Skan parameter β and select $f'(0) = u(0)/u_e$ as our independent parameter $a(X)$. At the junction point with the initial region of constant pressure, $a < 0$. At the rear stagnation point, $a = 0$; downstream of this point $a > 0$, and $a(X) \to 1$ as $X \to \infty$. The flow passes through a "throat" and goes supercritical downstream of the rear stagnation point, as in the Crocco-Lees[13] mixing theory. Calculations for adiabatic flow are now in progress. It also appears feasible to treat "cold" bodies, where the total enthalpy in the base flow region is initially lower than the freestream enthalpy.

References

[1] Prandtl, L., "Zur Berechnung der Grenzschichten," Z. Angew. Math. Mech. **18,** 77–82 (February 1938), transl. as NACA Tech. Memo. 959 (1940).

[2] Lees, L., "On the boundary layer equations in hypersonic flow and their approximate solutions," J. Aeronaut. Sci. **20,** 143–145 (1953).

[3] Hayes, W. D. and Probstein, R. F., *Hypersonic Flow Theory* (Academic Press, New York, 1959), Chap. IX.

[4] Ackeret, J., Feldmann, F., and Rott, N., "Investigations of compression shocks and boundary layers in gases moving at high speed," transl. as NACA TM 1113 (1947).

[5] Liepmann, H. W., "The interaction between boundary layer and shock waves in transonic flow," J. Aeronaut. Sci. **13,** 623–637 (1946).

[6] Oswatitsch, K. and Wieghardt, K., "Theoretical analysis of stationary potential flows and boundary layers at high speed," transl. as NACA Tech. Memo. 1189 (1948).

[7] Lees, L., "Interaction between the laminar boundary layer over a plane surface and an incident oblique shock wave," Princeton Univ., Aeronautical Engineering Lab., Rept. 143 (January 24, 1949).

[8] Chapman, D. R., Kuehn, D. M., and Larson, H. K., "Investigation of separated flows in supersonic and subsonic streams with emphasis on the effect of transition," NACA Rept. 1356 (1958).

[9] Gadd, G. E., "Boundary layer separation in the presence of heat transfer," AGARD Rept. 280 (April 1960).

[10] Curle, N., "The effects of heat transfer on laminar-boundary, layer separation in supersonic flow," Aeronaut. Quart. **XII,** 309–336 (November 1961).

[11] Honda, M., "A theoretical investigation of the interaction between shock waves and boundary layers," J. Aerospace Sci. **25,** 667–678 (1958).

[12] Abbott, D. E., Holt, M., and Nielsen, J. N., "Investigation of hypersonic flow separation and its effects on aerodynamic control characteristics," Vidya Rept. 81 (September 1962); also "Studies of separated laminar boundary layers at hypersonic speed with some low Reynolds number data," AIAA Paper 63-172 (June 17–20, 1963).

[13] Crocco, L. and Lees, L., "A mixing theory for the interaction between dissipative flows and nearly isentropic streams," J. Aeronaut. Sci. **19,** 649–676 (1952).

[14] Bray, K. N. C., Gadd, G. E., and Woodger, M., "Some calculations by the Crocco-Lees and other methods of interactions between shock waves and laminar boundary layers, including effects of heat transfer and suction," Aeronautical Research Council, Rept. 21, 834, FM 2937 (April 1960).

[15] Glick, H. S., "Modified Crocco-Lees mixing theory for supersonic separated and reattaching flows," Graduate Aeronautical Lab. California Institute of Technology Hypersonic Research Project Memo. 53 (May 2, 1960); also J. Aerospace Sci. **29,** 1238–1244 (1962).

[16] Sutton, W. G. L., "An approximate solution of the boundary layer equations for a flat plate," Phil. Mag. **23,** 1146–1152 (1937).

[17] Walz, A., "Anwendung des Energiesatzes von Wieghardt auf einparametrige Geschwindigkeitsprofile in laminaren Grenzschichten," Ing.-Arch. **16,** 243–248 (1948).

[18] Tani, I., "On the approximate solution of the laminar boundary layer equations," J. Aeronaut. Sci. **21,** 487–504 (1954).

[19] Stewartson, K., "Further solutions of the Falkner-Skan equation," Proc. Cambridge Phil. Soc. **50,** 454–465 (1954).

[20] Cohen, C. B. and Reshotko, E., "Similar solutions for the compressible laminar boundary layer with heat transfer and pressure gradient," NACA Rept. 1293 (1956).

[21] Hakkinen, R. J., Greber, I., Trilling, L., and Abarbanel, S. S., "The interaction of an oblique shock wave with a laminar boundary layer," NASA Memo. 2-18-59W (March 1959).

[22] Sterrett, J. R. and Emery, J. C., "Extension of boundary-layer separation criteria to a Mach number of 6.5 by utilizing flat plates with forward-facing steps," NASA TN D-618 (December 1960).

[23] Oswatitsch, K., "Die Ablösungsbedingung von Grenzschichten," *Symposium on Boundary Layer Research,* edited by H. Görtler (Springer-Verlag, Berlin 1958), pp. 357-367.

[24] Crocco, L., "Considerations on the shock-boundary layer interaction," Proceedings of the Conference on High-Speed Aeronautics, Polytechnic Institute of Brooklyn, pp. 75–112 (January 20–22, 1955).

[25] Crocco, L. and Probstein, R. F., "The peak pressure rise across an oblique shock emerging from a turbulent boundary layer over a plane surface," Princeton Univ., Aeronautical Engineering Dept., Rept. 254 (March 1954).

[26] Thwaites, B., "Approximate calculation of the laminar boundary layer," Aeronaut. Quart. **1**, 245–280 (November 1949).

[27] Rott, N. and Crabtree, L. F., "Simplified laminar boundary layer calculations for bodies of revolution and for yawed wings," J. Aeronaut. Sci. **19**, 553–565 (1952).

[28] Martellucci, A. and Libby, P. A., "Heat transfer due to the interaction between a swept planar shock wave and a laminar boundary layer," Proceedings of the USAF-ASD Symposium on Aeroelasticity, Dayton, Ohio (October 1960); also Aeronautical Systems Div.-TR-61-727, Vol. II (February 1962).

[29] Wieghardt, K., "Uber einen Energiesatz zur Berechnung laminarer Grenzschichten," Ing.-Arch. **16**, 231–242 (1948).

[30] Lees, L. and Reeves, B. L., "Some remarks on integral moment methods for laminar boundary layers with application to separation and reattachment," Graduate Aeronautical Lab., California Institute of Technology, Separated Flows Research Project, Rept. 1 (December 1961); also Air Force Office of Scientific Research Rept. 1920 (December 1961).

[31] Chapman, D. R., "Laminar mixing of a compressible fluid," NACA Rept. 958 (1950).

[32] Stewartson, K., "Correlated incompressible and compressible boundary layers," Proc. Roy. Soc. (London) **A200**, 84–100 (December 22, 1949).

[33] Savage, S. B., "The effect of heat transfer on separation of laminar compressible boundary layers," Graduate Aeronautical Lab., California Institute of Technology, Separated Flows Research Project, Rept. 2 (June 1962).

[34] Makofski, R., "A two-parameter method for shock wave-laminar boundary layer interaction and flow separation," *Proceedings of the 1963 Heat Transfer and Fluid Mechanics Institute* (Stanford University Press, Stanford, Calif., 1963), pp. 112–127.

[35] Lankford, J. L., "Investigation of the flow over an axisymmetric compression surface at high Mach numbers," Naval Ordnance Rept. 6866 (April 1960).

[36] Lankford, J. L., "The effect of heat transfer on the separation of laminar flow over axisymmetric compression surfaces," Naval Weapons Rept. 7402 (May 1961).

[37] Schaefer, J. W. and Ferguson, H., "Heat transfer and pressure distribution on cone-cylinder-flare configurations with boundary layer separation," NASA TN D-1436 (1962).